Proceedings of the 7th International Symposium on Cavitation
CAV2009 – Paper No. ##
August 17-22, 2009, Ann Arbor, Michigan, USA

Cavitation of JP-8 Fuel in a Converging-Diverging Nozzle: Experiments and Modelling

I. E. Dorofeeva
Graduate Research Assistant
University of Notre Dame
Notre Dame, IN, USA

F. O. Thomas
Professor
University of Notre Dame
Notre Dame, IN, USA

P. F. Dunn
Professor
University of Notre Dame
Notre Dame, IN, USA

ABSTRACT

This paper presents the results of an experimental investigation and an attempt to model cavitation of gas turbine aviation fuel. The work is motivated by the need to predict cavitation behavior for the design of modern aircraft fuel systems. Fuel cavitation can lead to unexpected degradation in system performance due to the effective compressibility associated with the formation of a two-phase mixture and/or damage of fuel system components due to subsequent bubble collapse. The primary working fluid for the experiments reported in this paper is JP-8, which is the gas turbine fuel most typically used by the United States military. JP-8 consists of over 228 hydrocarbons and is closely related to Jet A-1, which is the most common commercial gas turbine fuel. Experiments are also performed with dodecane and decane which are two of the primary constituents of JP-8 by weight but have disparate vapor pressures. Following the experimental study by Davis [7,8], a two-dimensional converging-diverging (C-D) nozzle geometry was selected for this experimental investigation. This relatively simple geometry is nonetheless capable of producing many of the essential features of fuel cavitation, including compressibility, choking, bubbly shock formation, and bubble collapse. In this paper, streamwise nozzle pressure distributions are presented for choked cavitating nozzle flows with water, JP-8, dodecane and decane the working fluids. An analytical model is developed which is shown capable of duplicating many essential features of the measured nozzle pressure distributions including streamwise location of a bubbly shock and the associated pressure jump.

INTRODUCTION

This paper presents the results of an investigation into fundamental aspects of cavitation in aviation fuel. The work is motivated by the need to predict cavitation behavior for the design of modern aircraft fuel systems. These systems are characterized by complex internal flow geometries that involve small passages and sharp turns, which lead to localized regions of high fluid velocity and low static pressure. Fuel cavitation can lead to unexpected degradation in system performance due to the effective compressibility associated with the formation of a two-phase mixture and/or damage of fuel system components because of subsequent bubble collapse.

The flow field geometry investigated in this paper is a simple converging-diverging (CD) nozzle. This comparatively simple geometry is convenient for the experimental characterization of fuel cavitation and also facilitates efforts toward the development of a fuel cavitation model. Both topics are addressed in this paper.

The primary working fluids for the experiments reported in this paper are JP-8, dodecane, decane and distilled water. JP-8 is the aviation fuel most commonly used by the United States military. It is a complex mixture of over 228 hydrocarbons and various additives to meet military specification MIL-DTL-83133 [1]. JP-8 is closely related to Jet A-1, which is the most common commercial aviation fuel. The primary difference is additives in JP-8 that are required for military applications. Details regarding the bulk fluid properties and the chemical composition of JP-8 can be found in reference [2]. Dodecane and decane represent large single component constituents of JP-8 by percent weight (22.54% and 16.08%, respectively) but possess very different vapor pressures (16Pa and 170 Pa, respectively). For comparative purposes, cavitation experiments are also performed using distilled water, because there have been previous studies in the literature regarding bubbly flow of water in C-D nozzles [3-6]. In contrast, with the exception of the recent work by Davis [7,8] there has been no work examining cavitation in aviation fuel. Davis [7,8] characterized the cavitation of JP-8 fuel in a C-D nozzle flow and made comparisons to the case of water cavitation. Measurements included high-speed digital imaging, streamwise static pressure distributions, non-intrusive void fraction and bubble velocity measurements. That work forms the background for the present study. The experimental results presented in this paper are obtained in the same experimental facility with the same C-D nozzle geometry. In [7,8] experiments were performed using JP-8 fuel, dodecane and distilled water as working fluids. The experimentally observed differences in the cavitating flow for these liquids were anticipated because of differences in bulk fluid properties.

The working fluids have vapor pressures that span three orders of magnitude: 2123 Pa for water (at 294 K), 170 Pa for

dodecane and 16 Pa for decane (both at 298 K]) [9]. The average vapor pressure of JP-8 fuel is 240 Pa [10]. Also it should be mentioned that the surface tension of water (7.2 mN) is more than three times that of JP-8 (2.3 mN), dodecane (2.5 mN) and decane (2.3 mN). This also has implications for both cavitation inception and bubble dynamics.

Here we present an extended experimental data set which also includes decane, in order to provide more information for comparative analysis. In addition we attempt to model the cavitation behavior observed in the experiments.

The primary objectives of this investigation are:

(1) To extend the experimental fuel cavitation experiments in a C-D nozzle reported by Davis [7,8]. In particular, nozzle static-pressure distributions for decane as the working liquid are obtained. As mentioned above, decane as well as dodecane is two main components of JP- 8 by percent weight but possess very different vapor pressures. Also, mass flow rate measurements are provided which are important for characterizing the choked flow regimes for this nozzle flow.

(2) To model the fuel cavitation as it occurs in JP-8 fuel, dodecane, decane and distilled water under identical C-D nozzle geometry and flow conditions. The model results are compared with the experimental results.

The paper is organized as follows: the experimental facilities are briefly described in the next section. This is followed by presentation of experimental results regarding pressure and mass flow rate measurements for JP-8, distilled water, dodecane and decane. The next section contains a description of the cavitation model. This is followed by the presentation of the fuel cavitation model results and comparison with the experiment.

EXPERIMENTAL FACILITY

The two-dimensional C-D nozzle used in this study was incorporated into a dedicated flow facility. The facility was designed to operate under reduced-pressure so that manageable flow rates of fuel (~3.8 L/min or ~1 gal/min) could be used in the test section. A schematic of the experimental facility is shown in Figure 1. This facility is essentially the same as that used by Davis [7,8] and only essential aspects are presented here. The reader is referred to Davis [7] for further details.

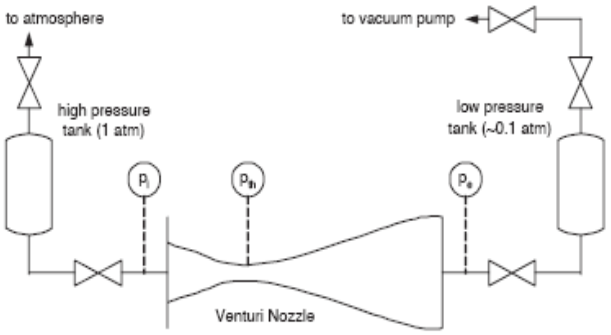

Figure 1: Schematic of the C-D nozzle cavitation facility (from Davis [7])

Two stainless steel, 38 L (10 gal) tanks served as liquid reservoirs. Initially, the upstream tank was filled with the working fluid for a particular experiment and was open to atmospheric pressure. The downstream tank was isolated from the system with a valve and was evacuated by a vacuum pump (Dekker Model RVL020W-01) to the desired back pressure, P_b. The back pressure was measured using a vacuum pressure gage (Dwyer Series SGL 4.5 in., 0 kPa to -100 kPa absolute, 1 % accuracy). The pressure differential between the upstream and downstream tanks drove the flow. Flow was initiated when the valves between the two tanks were opened and the upstream tank emptied through the C-D nozzle into the downstream tank. The volumetric flow rate of the liquid was measured using a flowmeter placed downstream of the nozzle test section (Dwyer type TVFS-02 Series, 0 gal/min to 1.2 gal/min, 2 % of full-scale accuracy).

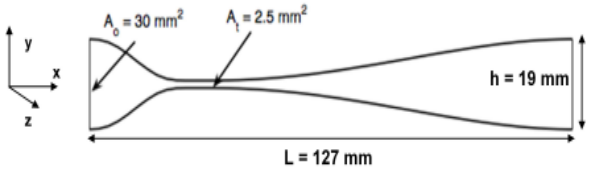

Figure 2: Schematic of the C-D nozzle geometry used for the experiments

A schematic of the nozzle geometry is shown in Figure 2. It is a channel of 1.6 mm depth with a rectangular cross section machined out of Plexiglas in the shape of a converging-diverging nozzle. Only two of the nozzle walls are contoured; the others are flat. The overall length of the nozzle, L, was 127 mm (5 in.). The nozzle throat area was constant from x = 25.4 mm (1.0 in.) to x = 31.8 mm (1.25 in.). The inlet and exit heights, h, were both 19 mm (0.75 in.), and the throat height was 1.59 mm (0.0625 in.). This gave a nozzle inlet-to-throat area ratio of 12:1. The streamwise and cross-stream spatial coordinates are denoted by x and y, respectively.

Local static pressures were measured using SETRA systems model 209 pressure transducers. Static pressure taps of 0.33 mm (0.0013 in.) in diameter were drilled normal to one flat nozzle wall along the centerline of the nozzle and were connected to the transducers using plastic tubing. Care was taken to ensure that this linear array of wall static pressure taps was hydrodynamically smooth. The taps were spaced at

intervals of 3.2 mm (0.125 in.) over the 12.7 cm (5 in.) length of the nozzle, resulting in 40 measurement locations. The pressures were acquired via a PC running LabView at a sampling frequency of 20 kHz. Pressure distributions at several different back pressures were acquired for the four working fluids.

Mass flow rate measurements were conducted to examine the effect of back pressure on the nozzle flow rate for all four fluids. These experiments identified the range of back pressures over which the mass flow rate through the nozzle was choked for each particular liquid.

EXPERIMENTAL RESULTS

In order to highlight differences in the character of cavitation as it occurs for each of the fluids investigated, Figures 3(a)-(d) present high-speed digital images (a frame rate of 6700 frames / sec) of nozzle cavitation for water, JP-8, dodecane and decane, respectively, for an imposed back pressure P_b = 0.2 kPa. In the water case (Figure 3 (a)) the bubble growth starts near the throat with initially spherical bubbles that grow quickly and coalesce into large vaporous voids. These subsequently undergo a rather sudden collapse in the diverging portion of the nozzle across a well defined bubbly shock wave. In the JP-8 fuel case (Figure 3 (b)) the bubbles that form near the nozzle throat do not merge to form large vapor voids but remain as a homogeneous mixture of smaller individual bubbles. Another obvious difference between water and JP-8 cavitation is the absence of a visually obvious bubbly shock in the fuel. In fuel the initial bubble growth phase is followed by a nearly homogeneous bubbly flow that seems to persist to the nozzle exit. Images taken for dodecane and decane are also shown in Figure 3 (c) and (d), respectively. While there is no visible bubbly shock for these liquids, the bubble size distribution in the diverging section of the nozzle is different than for JP-8 fuel case. The smallest bubbles that were present in the fuel appear to be gone for dodecane as well as for decane, and the bubble sizes appear to be larger for dodecane and considerably larger for decane.

a) water

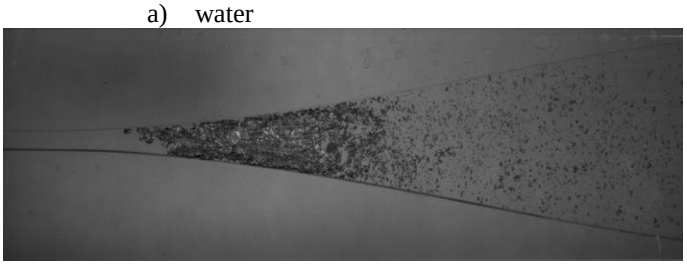

b) JP-8 fuel

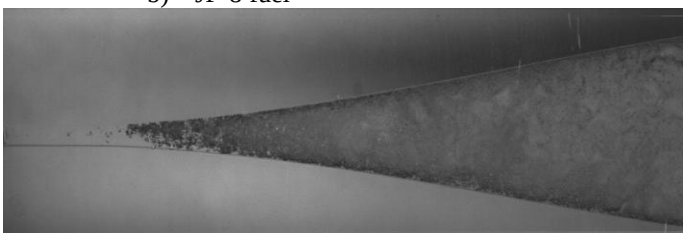

c) dodecane

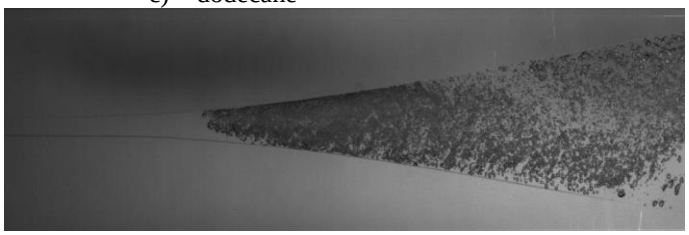

d) decane

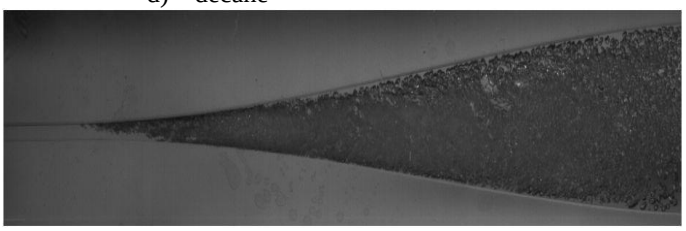

Figure 3: Images of a) water, b) JP-8, c) dodecane and d) decane cavitating mixtures. The tank back pressure for all cases was 20 kPa.

Measured mass flow rates as a function of imposed nozzle back pressure for water, JP-8, dodecane and decane are presented in Figure 4. This figure serves to establish the range of nozzle back pressures that result in choked flow due to the effective compressibility associated with cavitation. All four liquids exhibit similar behavior. As the back pressure is decreased the mass flow rate increases until the back pressure reaches a critical value and the nozzle chokes. Further reductions in back pressure have no effect on the mass flow rate through the nozzle. For the water case the critical back pressure is around 60 kPa. For JP-8 fuel, dodecane and decane it is approximately around 50 kPa.

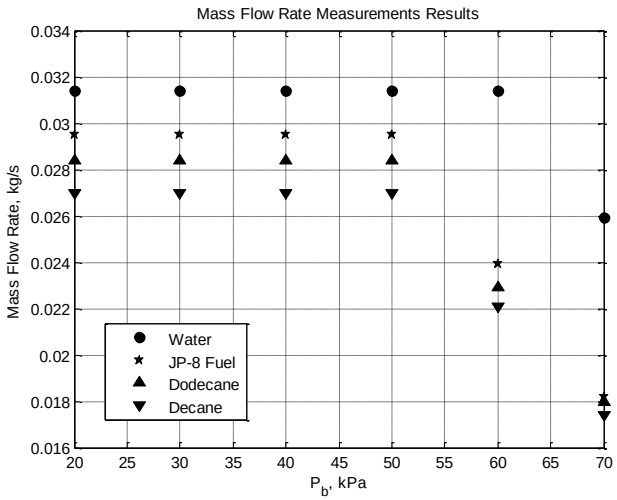

Figure 4: Measured mass flow rate as a function of receiver tank back pressure for water, JP-8 fuel, dodecane and decane

Measured streamwise pressure distributions for each fluid over a range of back pressures corresponding to choked flow (based on the results in Figure 4) are presented next. Figures 5-8 presents pressure distributions corresponding to nozzle back pressures of 46 kPa, 39kPa, 28kPa and 21kPa, respectively. This corresponds to pressure ratios, P_b / P_0 = 0.45, 0.38, 0.27

and 0.2. The streamwise static pressure distributions along the nozzle centerline are plotted versus non-dimensional axial position, x/L_{nozzle}, in each case. For reference, the nozzle geometry is superimposed on each figure.

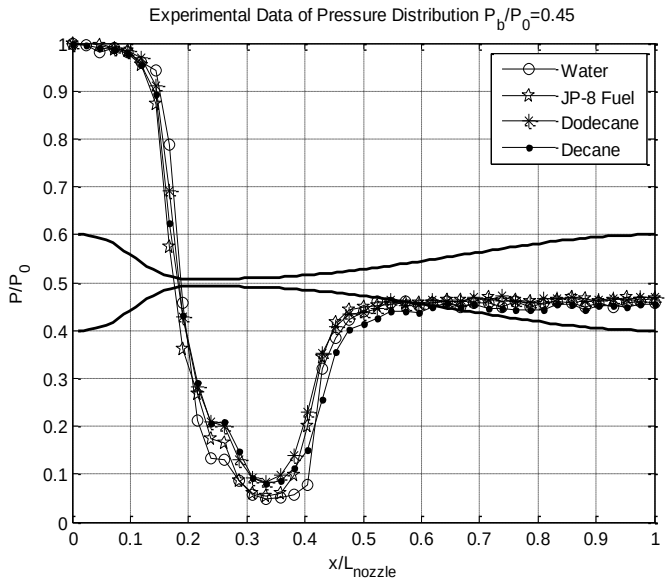

Figure 5: Pressure ratio measured along the centerline of the nozzle as a function of axial position for water, JP-8 fuel, dodecane and decane for back pressure ratio $P_b / P_0 = 0.45$.

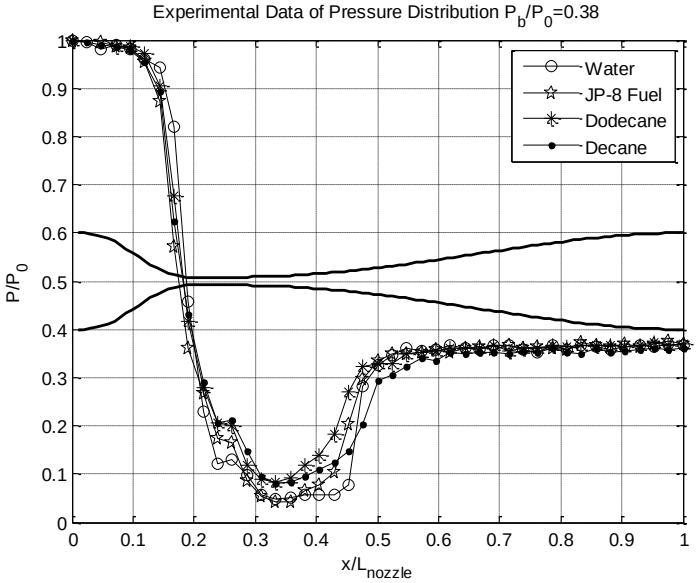

Figure 6: Pressure ratio measured along the centerline of the nozzle as a function of axial position for water, JP-8 fuel, dodecane and decane for back pressure ratio $P_b / P_0 = 0.38$.

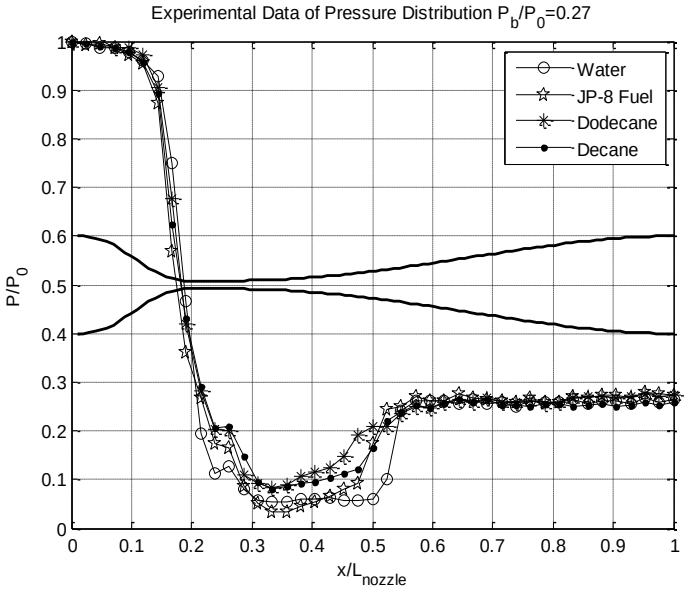

Figure 7: Pressure ratio measured along the centerline of the nozzle as a function of axial position for water, JP-8 fuel, dodecane and decane for back pressure ratio $P_b / P_0 = 0.27$.

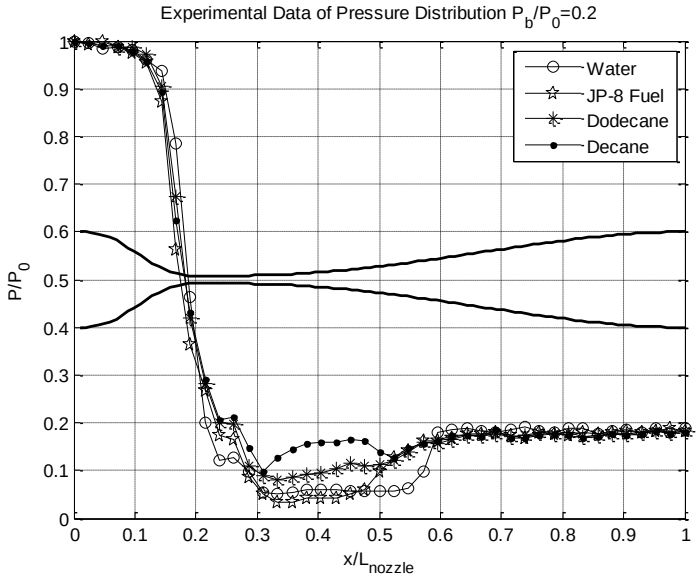

Figure 8: Pressure ratio measured along the centerline of the nozzle as a function of axial position for water, JP-8 fuel, dodecane and decane for back pressure ratio $P_b / P_0 = 0.2$.

The pressure profiles presented above are consistent with the choked flow condition. Note, for example, that the pressure continues to decrease (flow accelerates) downstream of the throat. The locally supersonic mixture terminates in a bubbly shock which is most evident in the case of water. The position of the shock moves downstream towards the exit as the back pressure is decreased. This behavior is consistent with gas dynamics. As the shock moves downstream in response to lower back pressure, however, the pressure jump across the shock is reduced; a behavior not consistent with flow of a compressible gas.

In spite of overall similarities in the general character of the pressure distributions, disparities do exist between the different fluids. The first significant difference to note is that each liquid reaches a unique value of pressure at the throat of the nozzle. This is likely related to issues regarding bubble growth in each case and the local void fraction at the throat (see [7,8]). The second difference involves the character of the pressure rise in the diverging portion of the nozzle. The differences between the pressure jump (bubbly shock structure) corresponding to each liquid increase with decreasing back pressure. For the case of pressure ratio $P_b / P_0 = 0.45$ (Figure 4) the pressure jump downstream of the throat is almost the same in each case. But for the case of $P_b / P_0 = 0.38$ (Figure 5) the pressure jump for water is noticeably sharper than the ones for JP-8 fuel, decane and dodecane. This difference between water and other liquids becomes more noticeable for cases of lower back pressure ratio $P_b / P_0 = 0.27$ (Figure 6) and $P_b / P_0 = 0.2$ (Figure 7). Obvious differences in the pressure jump are also evident in comparing dodecane, decane and JP-8 fuel. These differences are also more apparent at lower back pressure.

STEADY, BAROTROPIC, QUASI-1D MODEL

A steady, barotropic, quasi-one dimensional model is utilized to model the cavitating C-D nozzle flow. We consider a homogeneous, two-component mixture of gas and liquid in the absence of mass exchange and with no slip between phases. The mixture density is the sum of the density of the phases weighted according to their volume fractions.

$$\rho = \rho_l (1-\alpha) + \rho_g \alpha \tag{1}$$

The assumption of homogeneity allows treating the bubbly flow as a single-component flow. The flow is governed by continuity and inviscid momentum equations. The quasi-one-dimensional nozzle flow equations for the mixture take the form (see [11,12]):

$$\frac{d(\rho UA)}{dx} = 0 \tag{2}$$

$$U\frac{dU}{dx} = -\frac{1}{\rho}\frac{dp}{dx} \tag{3}$$

To close the above system of equations a barotropic relation between mixture pressure and gas void fraction is used:

$$\frac{p}{p_0} = \frac{\alpha_0(1-\alpha)}{\alpha(1-\alpha_0)} \tag{4}$$

The complete derivation of this barotropic equation of state for a bubbly mixture can be found in [11,12]. We assume that viscous and surface tension effects are negligible and that there is thermal equilibrium between the phases (equal local average phase temperatures). The liquid phase is assumed to be incompressible, while the gas phase is assumed to obey the ideal gas law. We do not include the effect of bubble dynamics.

The model formulated by equations (1)-(4) is qualitatively similar to one-dimensional gas dynamics. Results for isothermal, two-component flow were first detailed by Tangren [11] and more general results for any polytropic index by Brennen [12]. Those results were achieved with an assumption that both phases are always in dynamic equilibrium and do not include shock phenomenon. The C-D nozzle flow behavior of a bubbly mixture in dynamic equilibrium is similar to the isentropic expansion of an ideal gas through a C-D nozzle; there is subsonic flow in the convergent part of the nozzle and supersonic expansion in the divergent part.

The current experiments and those of Davis indicate the presence of bubbly shocks in the divergent part of the nozzle. In this paper we extend the model by the construction of a discontinuous nozzle flow solution with a normal shock in divergent part of the nozzle.

First, the solution for isothermal, barotropic two-phase nozzle flow in dynamical equilibrium throughout the nozzle is derived. Using (1), (2) and (4) we can rewrite equation (3) as follows

$$U\frac{\partial U}{\partial x} = \frac{p_0}{\rho_0}\frac{\alpha_0}{\alpha^2(1-\alpha)}\frac{\partial \alpha}{\partial x} \tag{5}$$

After integration of both sides of (5) from inlet velocity U_0 and initial void fraction α_0 we will come to the following:

$$U^2 = U_0^2 + \frac{2\alpha_0 p_0}{\rho_0}\left(\frac{1}{\alpha_0} - \frac{1}{\alpha} + \ln\left(\frac{(1-\alpha_0)\alpha}{(1-\alpha)\alpha_0}\right)\right) \tag{6}$$

The relation between the sonic speed of the barotropic two-phase mixture and gas void fraction is used here in the form

$$c^2 = \frac{p_0}{\rho_0}\frac{\alpha_0}{\alpha^2} \tag{7}$$

Using this relation we are able to apply equation (6) to the nozzle throat. Also for choked nozzle flow conditions we can use the fact that the local throat sonic speed is equal to the throat flow velocity.

$$c_{th}{}^2 = U_{th}{}^2 \tag{8}$$

Using equations (7) and (8), equation (6) takes the form,

$$\frac{p_0}{\rho_0}\frac{\alpha_0}{\alpha_{th}^2} = U_0^2 + \frac{2\alpha_0 p_0}{\rho_0}\left(\frac{1}{\alpha_0} - \frac{1}{\alpha_{th}} + \ln\left(\frac{(1-\alpha_0)\alpha_{th}}{(1-\alpha_{th})\alpha_0}\right)\right) \tag{9}$$

Using (2) and writing the inlet velocity in the form

$$U_0 = \left(\frac{\alpha_0 p_0}{\rho_0}\right)^{1/2}\frac{(1-\alpha_{th})A_{th}}{(1-\alpha_0)\alpha_{th}A_0} \tag{10}$$

and substituting (10) into (9), equation (9) can be solved to find a value for the void fraction at the throat α_{th} based on the initial void fraction α_0 and the throat area A_{th}. The inlet

velocity U_0 follows from (9), throat sonic speed c_{th} from (7) and the choked mass flow rate value $\dot{m}_{ch}$ is obtained from,

$$\dot{m}_{ch} = c_{th}\rho_{th}A_{th} = (p_0\rho_0)^{1/2}\frac{(1-\alpha_{th})\alpha_0^{1/2}}{\alpha_{th}(1-\alpha_0)}A_{th} \qquad (11)$$

Again by using continuity equation (2) we obtain the following relations,

$$U(x) = \frac{(1-\alpha_0)U_0A_0}{(1-\alpha(x))A(x)} \qquad (12)$$

And substituting (12) into (6) gives,

$$\frac{(1-\alpha_0)^2U_0^2A_0^2}{(1-\alpha(x))^2A(x)^2} = U_0^2 + \frac{2\alpha_0 p_0}{\rho_0}\left(\frac{1}{\alpha_0} - \frac{1}{\alpha(x)} + \ln\left(\frac{(1-\alpha_0)\alpha(x)}{(1-\alpha(x))\alpha_0}\right)\right) \qquad (13)$$

This algebraic equation can be solved numerically for void fraction distribution $\alpha(x)$ for a given nozzle geometry $A(x)$. Velocity $U(x)$, mixture density $\rho(x)$, pressure $p(x)$ and sonic speed $c(x)$ distributions along the nozzle can be found based on (12), (1), (4) and (7), respectively. In this manner a fully determined barotropic isothermal flow for given initial void fraction, α_0, and for a specified nozzle geometry is obtained. We need to emphasize here, that the solution is based on the assumption that the mixture is under dynamical equilibrium conditions all along the nozzle and the solution doesn't include discontinuities such as shocks. Note that exit pressure is not specified in the solution.

For nozzle flow containing a bubbly shock in the diverging portion of the nozzle, the solution outlined above is still valid from the inlet, through the throat and to the shock location in the diverging portion. Of course, the shock location is not known a priori, it is determined by the imposed nozzle back pressure.

To find the discontinuous shock solution we splice two barotropic continuous solutions achieved under the dynamical equilibrium assumption: one is the solution upstream of the shock previously described and the other is the 'post-shock' solution found based on the imposed nozzle exit condition (back pressure), exit void fraction and the value of choked mass flow rate. To splice these two solutions we apply the appropriate jump conditions from momentum conservation requirements and find the nozzle area where such a condition is satisfied. The assumption of dynamical equilibrium doesn't hold at this point; the shock is a non-equilibrium process, but the equilibrium assumption is true at all other streamwise locations.

From barotropic relation (4) we find the void fraction at the exit of the nozzle corresponding to the imposed back pressure,

$$\alpha_b = \frac{\alpha_0}{p_b(1-\alpha_0)/p_0 + \alpha_0} \qquad (14)$$

Based on (2) and the previously determined choked mass flow rate we have,

$$U_b = \frac{\dot{m}_{ch}}{\rho_b A_b} = \frac{\dot{m}_{ch}(1-\alpha_0)}{\rho_0(1-\alpha_b)A_b} \qquad (15)$$

Using (14) and (15) we obtain a "post shock" equation analogous to (13),

$$\frac{(1-\alpha_b)^2U_b^2A_b^2}{(1-\alpha(x))^2A(x)^2} = U_b^2 + \frac{2\alpha_0 p_0}{\rho_0}\left(\frac{1}{\alpha_b} - \frac{1}{\alpha(x)} + \ln\left(\frac{(1-\alpha_b)\alpha(x)}{(1-\alpha(x))\alpha_b}\right)\right) \qquad (16)$$

We denote conditions upstream of the shock by subscript 1 and downstream by subscript 2. With assumptions of the infinitely small shock thickness we can use the jump condition coming from (2) in form of

$$\rho_1(x_{sh})U_1^2(x_{sh}) + p_2(x_{sh}) = \rho_2(x_{sh})U_2^2(x_{sh}) + p_2(x_{sh}) \qquad (17)$$

where x_{sh} denotes the location of the shock where condition (17) is satisfied.

Figure 9 illustrates an example of the solution constructed by this method and shows the pressure distribution along the nozzle. We have a fully determined barotropic isothermal flow with the stationary normal shock wave found for specific inlet parameters, exit conditions and particular nozzle geometry**.** Although not discussed in this paper it should be mentioned that by solving the same model equations, but in a time dependent formulation using shock capturing techniques, numerical solutions in agreement with the present model results have also been obtained.

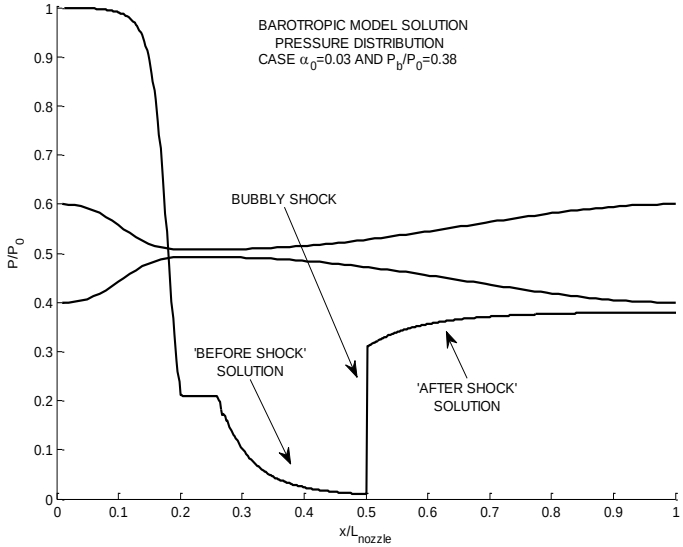

Figure 9: Example of steady, barotropic quasi-1D model solution for pressure distribution for the experimental nozzle geometry.

MODEL RESULTS

Before presenting the model results, some comments are in order regarding the choice of the nozzle inlet void fraction, α_0, for a particular liquid. In the experiments, initial void fraction is manifest through the presence of trapped pockets of undissolved gas on microparticle impurities or cracks and pits along the walls of the test section apparatus [7,8]. The role of solid impurities acting as cavitation nuclei has been studied extensively in the literature [13-15].

We can make inferences about approximate values of initial void fraction for a particular cavitating liquid based on the barotropic model approach. Measurable nozzle choked flow parameters such as pressure at the throat and choked mass flow

rate can provide the basis for initial void fraction estimates. Based on equations (9) and (4) we can find the dependence of the throat pressure on the initial void fraction as was the case in [11,12]. Figure 10 shows the analytical dependence of the throat to inlet pressure ratio versus initial void fraction. On this analytical curve experimentally measured values of pressure at the throat corresponding to the choked regime for each working fluid are indicated. If we assume that the cavitating nozzle flow is well described by the barotropic model, then, from Figure 10, we can estimate the approximate values of initial void fraction α_0 for each working liquid.

We can also repeat the same procedure as outlined above, but utilize measured values of the choked mass flow rate. Figure 11 shows a plot of the dependence of choked mass flow rate upon the initial void fraction from equations (9) and (11). Experimental values of choked mass flow rate are superimposed on the analytical curve. Assuming the validity of the barotropic model, it is possible to estimate the initial void fraction values for each fluid based on their choked mass flow rate values.

Both procedures yield estimates of initial void fraction for water that are fully consistent. For JP-8, dodecane and decane there are discrepancies but these are within the experimental uncertainties of the measurements on which they are based. The estimated values of initial void fractions used in the model for water, JP-8 fuel and dodecane are α_0 = 0.008, 0.02 and 0.03, respectively.

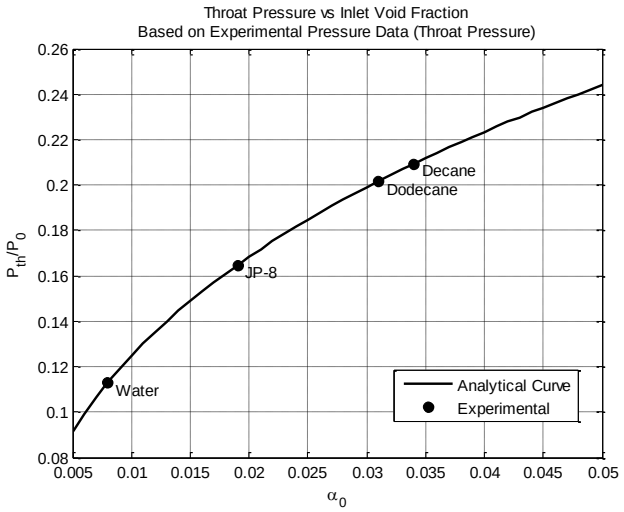

Figure 10: Analytical dependence of the throat to inlet pressure ratio versus initial void fraction. Experimentally measured values of pressure at the throat corresponding to the choked regime for each working fluid are indicated.

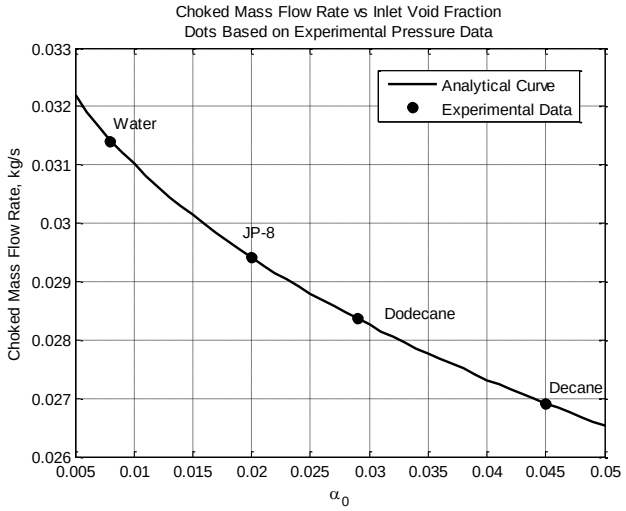

Figure 11: Analytical dependence of choked mass flow rate upon the initial void fraction. Experimental values of mass flow rates corresponding to the choked regime for each working fluid are indicated.

Figures 12-14 compare computed and measured nozzle pressure distributions for different imposed nozzle back pressures that correspond to choked nozzle flow. In each figure, results for water, JP-8 and dodecane are shown. The initial void fractions appropriate for each fluid (as previously described) have been used for the model results. For each liquid, the model solution is in a good agreement with experimental results in the convergent part of the nozzle. The barotropic model solutions also reproduce the flow behavior at the nozzle throat for all liquids and in the divergent part of the nozzle downstream of the shock location. The barotropic model results show that the shock location moves upstream with increasing values of the back pressure. This behavior is fully consistent with experimental observation. The modeled pressure distributions capture the bubbly shock location observed in the experiment as well as the magnitude of the pressure jump. This bubbly shock is most apparent in the experiments with water. The effect of initial void fraction on the modeled shock location appears to be negligible, however.

The greatest disparity between measured and modeled pressure distributions concerns the structure of the pressure rise across the shock. For each working fluid the measured pressure rise across the shock is not as spatially localized as the model would indicate. The most localized shock occurs in the water experiments and the most gradual pressure rise occurs for dodecane. Note also that the shock structure in experiments has a tendency to be more smeared as back pressure is reduced. Obviously, the barotropic model does not predict such complex shock wave behavior. This may be due to the model assumption of homogeneous mixture flow in dynamic equilibrium which may be violated in the shock region. Such physical phenomenon as bubble dynamics, bubbles transport with slip and bubble-bubble interaction could play the significant role at this particular region of the shock structure location [16-23].

Figure 15 summarizes JP-8 pressure distributions predicted by the barotropic model and compares them with experiments at three imposed back pressures. These solutions are achieved with the same previously assumed value of initial void fraction corresponding to JP-8 fuel. The model closely reproduces the measured pressure in the convergent part of the nozzle and throat. The barotropic solution also predicts the strength of the pressure rise across the shock. It is interesting to note that the shock location predicted from the barotropic model corresponds to the end of the pressure rise in the JP-8 fuel experiments. The barotropic model fails to reproduce the smeared structure of the shock wave which seems to be inherent in JP-8 fuel cavitation. One of the simplest ways to simulate the smeared shock structure in JP-8 fuel and dodecane within the context of the barotropic model would be to include a fluid specific effective viscosity term that would have the effect of diffusing the shock location. This approach is currently under investigation.

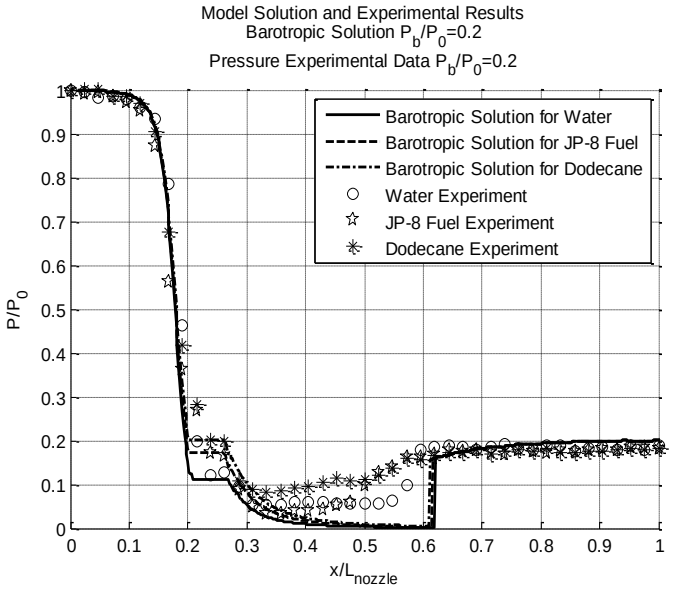

Figure 12: Comparison of measured pressure ratio distributions for water, JP-8 fuel and dodecane for $P_b / P_0 = 0.2$ and modeled pressure ratio distributions for $P_b / P_0 = 0.2$ at three cases of specified initial void fractions.

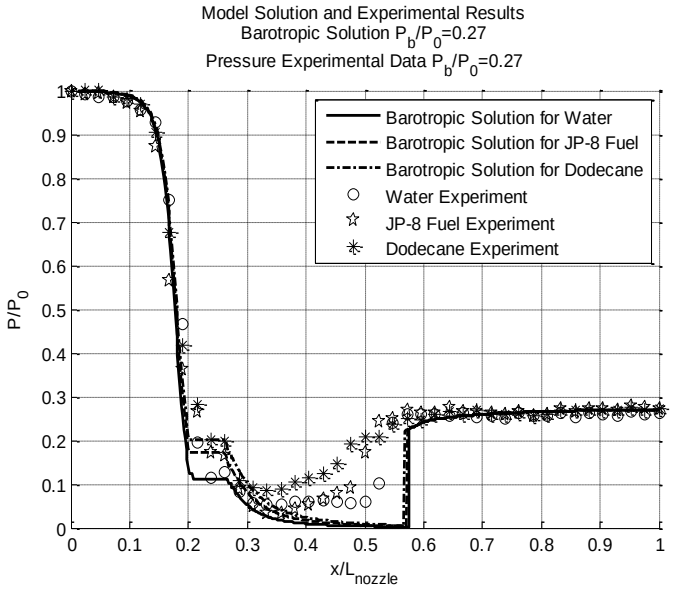

Figure 13: Comparison of measured pressure ratio distributions for water, JP-8 fuel and dodecane for $P_b / P_0 = 0.27$ and modeled pressure ratio distributions for $P_b / P_0 = 0.27$ at three cases of specified initial void fractions.

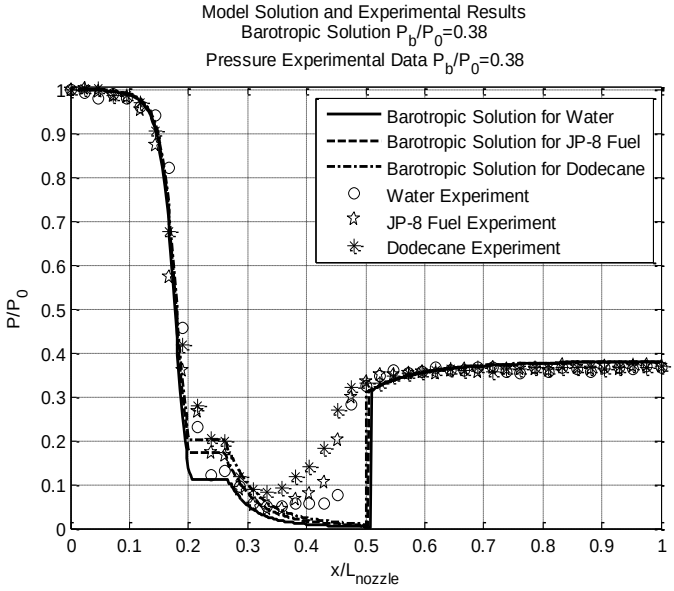

Figure 14: Comparison of measured pressure ratio distributions for water, JP-8 fuel and dodecane for $P_b / P_0 = 0.38$ and modeled pressure ratio distributions for $P_b / P_0 = 0.38$ at three cases of specified initial void fractions.

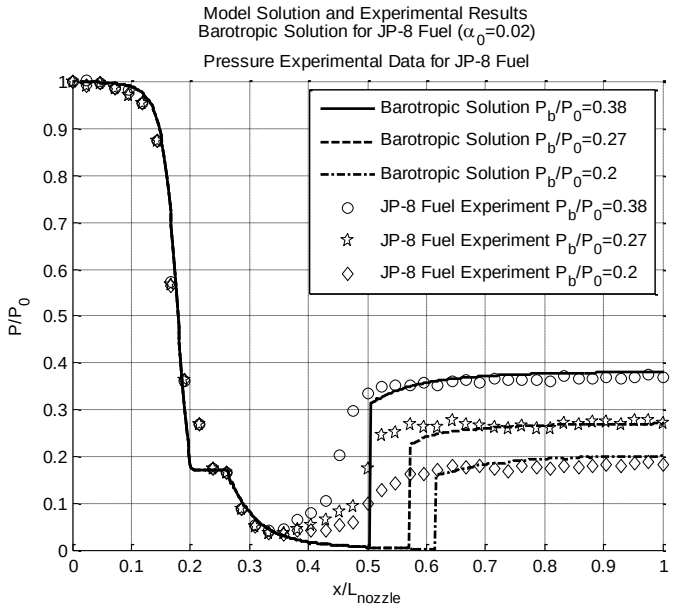

Figure 15: Comparison of measured pressure ratio distributions for JP-8 fuel and modeled pressure ratio distributions at specified $\alpha_0 = 0.02$ for three cases of imposed back pressure ratios**.**

CONCLUSION

The fuel cavitation experiments in a C-D nozzle reported by Davis [7,8] were extended in this work by considering decane as an additional one-component surrogate of aviation fuel. The nozzle static-pressure distributions for water, JP-8 fuel, dodecane and decane are presented. Mass flow rate measurements for obtained in each case for various nozzle pressure ratios established choked flow regimes for each case. The experiments together with those of Davis [7,8] indicate the presence of bubbly shocks in the divergent part of the nozzle.

A steady, barotropic, quasi-one dimensional model with discontinuous nozzle flow solution corresponding to a normal shock in the divergent part of the nozzle was developed to simulate the cavitating C-D nozzle flow. Measurable nozzle choked flow parameters such as pressure at the throat and choked mass flow rate were used to provide the basis for initial void fraction estimates for each working liquid. Comparison between the computed and measured nozzle pressure distributions for different imposed nozzle back pressures corresponding to the choked nozzle flow regime was presented for JP-8 fuel as well as dodecane and water.

It is demonstrated for each of the liquids that the barotropic model solutions reproduce the pressure distributions in the convergent part of the nozzle, the nozzle throat and also in divergent part of the nozzle just downstream of the shock location. The barotropic solution also predicts the bubbly shock location as well as the pressure rise across the shock. It was shown that the modeled shock location moves upstream with increasing values of the back pressure which is fully consistent with experimental observation. The effect of initial void fraction on the modeled shock location appeared to be negligible. Based upon the measurements of Davis [8] this does not appear to be the case.

The greatest disparity between the model results and experiments is in capturing the spatial extent over which the pressure rise occurs across the bubbly shock. The best agreement is with water where the shock is most pronounced both visually and spatially localized in the pressure measurements. In the case of JP-8, dodecane and decane the pressure rise occurs over a more extended streamwise region (i.e. the shock appears "smeared") and the model in its present form does not capture this behavior. It is interesting to note, however, that for JP-8 and dodecane the shock location predicted by the model is where the pressure rise for these liquids is complete and the final pressure rise is also well predicted. In order to simulate the smeared JP-8 fuel and dodecane shock structure behavior, it may be possible to augment the model with a fluid specific effective viscosity that would have the effect of diffusing the shock location.

ACKNOWLEDGMENTS

This research was supported by Honeywell Aerospace. We especially thank Steve Emo, Corey Bourassa and Abigail Parsons for their numerous technical interactions and support.

NOMENCLATURE

α	Void fraction ($\alpha = \frac{volume\ \ of\ \ gas}{total\ \ volume}$)
ρ	Mixture density ($\rho = \rho_l(1-\alpha) + \rho_g \alpha$)
ρ_l	Liquid phase density ($\rho_l = const$)
ρ_g	Gas phase density ($\rho_g = \rho_{g0} \frac{p}{p_0}$)
p	Pressure of the mixture
U	Axial velocity of the mixture
c	Speed of sound for two phase mixture
A	Cross sectional area of the nozzle
x	Nozzle axial coordinate
x_{sh}	Coordinate of shock location
$\dot{m}_{ch}$	Choked mass flow rate

Subscript

0	Nozzle inlet conditions
th	Nozzle throat conditions
b	Nozzle exit conditions

REFERENCES

[1] Mayfield, H. T., 1996. *JP-8 Composition and Variability*, Report No.AL/EQ-TR-1996-0006, Armstrong Laboratory, Environ. Res. Div., Tyndall Air Force Base, FL.

[2] *Handbook of Aviation Fuel Properties*, 2004, 3rd Ed., Coordinating Research Council, Inc.

[3] Muir, J. F., and Eichhorn, R., 1963. "Compressible Flow of an Air-Water Mixture through a Vertical, Two Dimensional Nozzle," *Proc. 1963 Heat Trans. and Fluid Mech. Inst.*, 183-204.

[4] Sandhu, N., and Jameson, G. J., 1979. "An Experimental Study of Choked Foam Flows in a Convergent-Divergent Nozzle," *Int. J. Multiphase Flow* 5, 39-58.

[5] Thang, N. T., and Davis, M. R., 1981. "Pressure Distribution in Bubbly Flow Though Venturis," *Int. J. Multiphase Flow* 7, 191-210.

[6] Ishii, R., Umeda, Y., Murata, S., and Shishido, N., 1993. "Bubbly flows through a Converging-Diverging Nozzle," *Phys. of Fluids* A 5, 1630-1643.

[7] Davis, M., 2008, "Experimental Investigation of the Cavitation of Aviation Fuel in a Converging-Diverging Nozzle," Ph.D. dissertation, University of Notre Dame

[8] Dunn, P., Thomas, F. O. & Davis, M. P., 2009. "Experimental Investigation of Aviation Fuel Cavitation in a Converging-Diverging Nozzle," *Int. J. Multiphase Flow*, in review.

[9] Mackay, D., Shiu, W.Y., and Ma, K.C., 1993. *Illustrated Handbook of Physical-Chemical Properties and Environmental Fate for Organic Chemicals*, Volume III: Volatile Organic Chemicals, Lewis Publishers, Ann Arbor, MI.

[10] *JP-8 Volatility Study*, 2001. Report No. IERA-RS-BR-SR-2001-0002, Southwest Research Institute, San Antonio, TX.

[11] Tangren, R. F., Dodge, C. H., and Seifert, H. S., 1949. "Compressibility Effects in Two-Phase Flow," *J. Appl. Phys*. 20, 637-645.

[12] Brennen, C. E., 2005. *Fundamentals of Multiphase Flow*. Cambridge Univ. Press.

[13] Robert E. Apfel., 1970, The Role of Impurities in Cavitation - Threshold Determination. *The Journal of the Acoustical Society of America*, 48(5):1179–1186.

[14] Knud A. Morch., 2000, "Cavitation Nuclei and Bubble Formation - A Dynamic Liquid-Solid Interface Problem," *Trans. ASME*, 122:494–498.

[15] H. B. Marschall and K. A. Morch., 2003, "Cavitation inception by almost spherical solid particles in water," *Phys. of Fluids*, 15(2):545–553.

[16] Wang, Y-C., and Brennen, C. E., 1998, "One-Dimensional Bubbly Cavitating Flows Through a Converging-Diverging Nozzle," *Trans. ASME* 120, 166-170.

[17] Preston, A. T., Colonius, T., and Brennen, C. E., 2002, "A Numerical Investigation of Unsteady Bubbly Cavitating Nozzle Flows," *Phys. of Flu*ids 14, 300-311.

[18] Delale, C. F., Schnerr, G. H., and Sauer, J., 2001, "Quasi-One-Dimensional Steady-State Cavitating Nozzle Flows," *J. Fluid Mech*. 427, 167-204.

[19] Delale, C. F., Okita, K., and Matsumoto, Y., 2005. "Steady-State Cavitation Nozzle Flows with Nucleation," *Trans. ASME* 127, 770-777.

[20] L. van Wijngaarden, 1972, "One-dimensional flow of liquids containing small gas bubbles," *Ann. Rev. Fluid Mech.* 4, 369-396.

[21] L. Noordzij and L. van Wijngaarden, 1974, "Relaxation effects, caused by relative motion, on shock waves in gas-bubble/liquid mixtures," *J. Fluid Mech*. 66, 115-144.

[22] R.I. Nigmatulin and V.Sh. Shagapov, 1976, "Structure of shock waves in a liquid containing gas bubbles," *Fluid Dynamics* 9, 890-899.

[23] M. Kameda, N. Shimaura, F. Higashino, and Y. Matsumoto. 1998, "Shock waves in a uniform bubbly flow," *Phys. of Fluids* **10**, 2661.